Available online at www.sciencedirect.com
SCIENCE DIRECT®
Optics Communications 219 (2003) 101–116
OPTICS COMMUNICATIONS
www.elsevier.com/locate/optcom

# High range resolution velocity estimation techniques taking into account the frequency chirp in coherent Doppler lidars

Ljuan L. Gurdev*, Tanja N. Dreischuh

*Institute of Electronics, Bulgarian Academy of Sciences, 72 Tzarigradsko Shosse Blvd., BG-1784 Sofia, Bulgaria*

Received 24 July 2001; received in revised form 16 February 2003; accepted 16 February 2003

**Abstract**

Taking into account the sensing-pulse frequency chirp, we have derived generalized algorithms for recovering the non-uniform Doppler-velocity coherent-lidar profiles within the lidar resolution interval conditioned by the pulse length. The laser pulses are assumed to have an exponentially shaped form. The performance and the efficiency of the algorithms obtained are studied and illustrated by computer simulations. It is shown that in the presence of arbitrary, in form and magnitude, but known regular frequency chirp, at some reasonable number of signal realizations and appropriate data processing to suppress the noise effects, the Doppler-velocity profiles can be determined accurately with considerably shorter resolution scale compared with the pulse length.


*PACS:* 42.68.Wt.; 42.79.Qx

*Keywords:* Lidar remote sensing; Coherent Doppler lidar; Intrapulse frequency chirp

## 1. Introduction

Pulsed coherent Doppler lidars are of considerable contemporary interest as an effective tool for contactless remote sensing of atmospheric wind. The laser sources that are most frequently used in this lidars operate at wavelengths $\lambda$ of 10.6 μm ($CO_2$ lasers [1–4]) and 2 or 2.1 μm (some solid-state lasers [4–6]).

There are at least two approaches for improving the range resolution of pulsed coherent Doppler lidars. Such a first approach is based on the conception that the minimum achievable range resolution cell is of the order of the sensing laser pulse length (see, e.g. [1,7]). On the other hand, the laser pulse length is reciprocally related with an uncertainty in the determination of the Doppler velocity [8]. Thus, in this case, the

* Corresponding author.
*E-mail address:* lugurdev@ie.bas.bg (L.L. Gurdev).

0030-4018/03/$ - see front matter 
doi:10.1016/S0030-4018(03)01292-6

range resolution cell and the Doppler-velocity uncertainty are reciprocally related. But so far as their product is proportional to the wavelength of the laser radiation [8], one can improve the range resolution without lowering the velocity sensitivity, by using shorter sensing pulses of shorter-wavelength laser radiation. Such is the case of using laser pulses with wavelength $\lambda = 2$ μm instead of five times longer pulses with $\lambda = 10.6$ μm.

Another approach is to develop inverse mathematical techniques (algorithms) for retrieving the Doppler-velocity profiles with considerably shorter resolution cell compared with the pulse length. Based on the analysis of the complex heterodyne signal autocovariance, we have developed recently such techniques concerning the cases of rectangular [9] and exponentially shaped [10] laser pulses. The results obtained in [9,10] are strictly valid under the condition that the effect of the frequency chirp in the sensing laser pulses is negligible. We consider as *chirp* the regular (mean) intrapulse frequency deviation that is reproducible from pulse to pulse. The random (stationary) frequency fluctuations have been considered formerly [10]. In many cases (see, e.g. [1,6]) the regular and random frequency deviations are so small that their neglect would not lead to noticeable error in the determination of the Doppler-velocity profiles. That is, the error would be much less for instance than one meter per second. In other cases the frequency deviations can have large values corresponding to seeming velocity variations of many meters per second [1,11–15]. Such variations exceed the mean retrieval error caused for instance by turbulent velocity fluctuations [10]. Then one should take into account the influence of the frequency deviations on the accuracy of the Doppler-velocity profiles obtained on the basis of various Doppler-velocity estimators.

Although the chirp effect is apparently more important in the $CO_2$ coherent Doppler lidars, according to the available literature data [11–15], it may also be noticeable in coherent lidars with solid-state laser transmitters [16]. In any case, one should estimate the error in the determination of the Doppler-velocity profiles caused by the neglect of the frequency chirp in the corresponding velocity estimation techniques (estimators, algorithms). When the error has unacceptable large value one should modify the known algorithms in such a way that to take into account and eliminate the chirp effect on the final results. For instance, in [17] it is shown how to remove a typical chirp-due bias error in the Doppler-velocity profiles obtained on the basis of $CO_2$ coherent lidar data by using PP frequency estimator [18,19].

A purpose of the present work is to investigate (Section 4) the character of the error due to the neglect of the frequency chirp, when recovering high-resolution Doppler-velocity profiles by using the inverse algorithms developed in [10]. The main purpose of the work is to develop new more general inverse techniques for retrieving high-resolution Doppler-velocity profiles (Section 3), taking into account (and thus correcting for) the frequency chirp in the coherent-lidar sensing pulses. The pulse power shape and the temporal behaviour of the regular frequency deviation are supposed to be known. They can, in principle, be determined experimentally [11–15] or predicted theoretically [13,14]. Here we consider the case of exponentially shaped sensing laser pulses that can be good approximations of real asymmetric laser pulses generated by various solid-state and $CO_2$ lasers (see, e.g. [10,11,20–25].

The new algorithms are obtained on the basis of an analysis of a general expression of the complex heterodyne signal autocovariance that is given in Section 2. The algorithm performance and efficiency are studied and illustrated by computer simulations in Section 4.

## 2. Complex heterodyne signal autocovariance

The aerosol single-scattering complex heterodyne lidar signal $I(t) = J(t) + iQ(t)$ is in general a nonstationary random process whose autocovariance $\mathrm{Cov}(t,\theta) = \langle I^*(t)I(t+\theta)\rangle$ depends not only on the time shift $\theta$ but on the moment $t$ as well; $J(t)$ and $Q(t)$ are inphase and quadrature components, respectively, ensemble average is designated by $\langle\cdot\rangle$, i is imaginary unity, and the superscript $*$ denotes complex

conjugation. For a positive time shift $\theta \geqslant 0$ we have obtained in [10], the following expression of the autocovariance function:

$$\mathrm{Cov}(t,\theta) = \int_{z_0}^{ct/2} \mathrm{d}z' f_{\mathrm{m}}(t-2z'/c) f_{\mathrm{m}}(t+\theta-2z'/c)\eta(\vartheta = t-2z'/c,\theta)\Phi(z') \times \exp\{\mathrm{i}[\omega_{\mathrm{m}}(z')\theta + \delta\omega_{\mathrm{ch}}[(t-2z'/c)\chi(z')]\theta\chi(z')]\}\zeta[\theta\chi(z')]\xi[\theta\chi(z')]\gamma(z', 2\omega_0\theta/c), \quad (1)$$

where $z_0$ is the upper limit of the lidar dead (blind) zone (the radiation backscattered from this zone is not detectable); $z = ct/2$ is the position (along the lidar line of sight) of the pulse front corresponding to the moment of detection $t$ (after the pulse emission), $c$ is the speed of light; $z'$ is a current longitudinal coordinate along the line of sight; $f_{\mathrm{m}}(\vartheta)$ is the ensemble-mean shape of the pulse envelope $f_0(\vartheta) = f_{\mathrm{m}}(\vartheta)[1+g(\vartheta)]$, $g(\vartheta) = [f_0(\vartheta) - f_{\mathrm{m}}(\vartheta)]/f_0(\vartheta)$ describes the relative pulse-shape fluctuations, $\langle g(\vartheta)\rangle = 0$, and, respectively, $\langle f_0(\vartheta)\rangle = f_{\mathrm{m}}(\vartheta)$, $\langle f_0(\vartheta) f_0(\vartheta+\theta)\rangle = f_{\mathrm{m}}(\vartheta) f_{\mathrm{m}}(\vartheta+\theta)\eta(\vartheta,\theta)$, $\eta(\vartheta,\theta) = 1 + \mathrm{Cov}_g(\vartheta,\theta)$, and $\mathrm{Cov}_g(\vartheta,\theta) = \langle g(\vartheta)g(\vartheta+\theta)\rangle$ is the autocovariance of $g(\vartheta)$; $\Phi(z')$ is proportional to the mean short-pulse ($\delta$-pulse) signal power profile [9,10] and characterizes the contribution to the mean signal power of unitary "scattering length" along the line of sight; $\omega_{\mathrm{m}}(z') = \omega_0\chi(z') - \omega_{\mathrm{h}}$ is the intermediate frequency, $\omega_0$ is the basic frequency of the sensing pulsed radiation, $\omega_{\mathrm{h}}$ is the optical heterodyne frequency, $\chi(z') = 1 - 2v(z')/c$, $v(z')$ is the ensemble-mean profile of the radial (Doppler) velocity of the aerosol scatterers; $\delta\omega_{\mathrm{ch}}(\vartheta)$ is the regular frequency deviation (chirp), with respect to $\omega_0$, in the sensing laser pulses; and $\zeta[\theta\chi(z')] = \langle\exp[\mathrm{i}\delta\omega_{\mathrm{r}}\theta\chi(z')]\rangle$, $\xi[\theta\chi(z')] = \langle\exp[\mathrm{i}\varphi_{\mathrm{r}}^{\mathrm{I}}\theta\chi(z')]\rangle$, and $\gamma(z', 2\omega_0\theta/c) = \langle\exp[\mathrm{i}2\omega_0\theta\tilde{v}(z')/c]\rangle$ are real characteristic functions supposed to characterize, respectively, symmetrically distributed zero-mean frequency fluctuations $\delta\omega_{\mathrm{r}}(\vartheta)$ and (differentiated realizations $\varphi_{\mathrm{r}}^{\mathrm{I}}(\vartheta)$ of) phase fluctuations $\varphi_{\mathrm{r}}(\vartheta)$ in the sensing laser pulse, and radial velocity fluctuations $\tilde{v}(z')$ along the line of sight. The random functions $\delta\omega_{\mathrm{r}}(\vartheta)$ and $\varphi_{\mathrm{r}}(\vartheta)$ [$\varphi_{\mathrm{r}}^{\mathrm{I}}(\vartheta)$] are considered as statistically stationary and independent of each other and, certainly, of the velocity fluctuations $\tilde{v}(z')$. When deriving Eq. (1) we have supposed [10] that the phase terms $\varphi_{\mathrm{ch}}(\vartheta) = \int_0^{\vartheta}\delta\omega_{\mathrm{ch}}(t')\,\mathrm{d}t'$ (phase increment due to the chirp), $\varphi_{\omega r}(\vartheta) = \int_0^{\vartheta}\delta\omega_{\mathrm{r}}(t')\,\mathrm{d}t'$ (phase increment due to the random frequency fluctuations), and $\varphi_{\mathrm{r}}(\vartheta)$ (other possible phase fluctuations) change slowly enough within time intervals $T$ of the order of $\theta$ so that $\varphi(\vartheta+T) - \varphi(\vartheta) \cong \varphi^{\mathrm{I}}(\vartheta)T$; here the superscript I denotes differentiation with respect to $\vartheta$.

Let us also briefly consider the question about the formation of the characteristic function $\gamma(z', 2\omega_0\theta/c)$ in Eq. (1) in the case of turbulent velocity fluctuations $\tilde{v}(z')$. In practice, the signal autocovariance estimate is obtained by averaging over some number $N$ of conjecturally independent signal realizations obtained (by $N$ laser shots) for an accumulation period (observation time) $T_{\mathrm{a}}$. Within $T_{\mathrm{a}}$ the fast varying [small temporal (and spatial) scale] turbulent velocity fluctuations are averaged (together with the speckle and other random phase fluctuations), taking part in this way in the formation of the corresponding characteristic function $\gamma(z', 2\omega_0\theta/c)$ in Eq. (1). The small-scale fluctuations are weak as compared with the slowly varying [large temporal (and spatial) scale] velocity fluctuations that are not averaged and take part in the formation of a mean for the period $T_{\mathrm{a}}$, but range-resolved velocity profile $v(z')$ [Eq. (1)]. For a long enough observation time $T_{\mathrm{a}}$ (e.g., of the order of minutes) that exceeds essentially the mean correlation time $\tau_{\mathrm{cv}}$ of the fluctuation process ($T_{\mathrm{a}} \gg \tau_{\mathrm{cv}}$) one will obtain a long-term average velocity profile $v(z')$ and a full-variance characteristic function $\gamma(z', 2\omega_0\theta/c)$ resulting from averaging all the velocity fluctuations. Under stationary conditions, the profile $v(z')$ obtained in this case is an estimate of the parent population mean velocity profile. Under non-stationary conditions, when there are appreciable trends, the long-term averaging is characterized by low temporal resolution. When the value of $T_{\mathrm{a}}$ is small (e.g., of the order of a few seconds) in comparison with $\tau_{\mathrm{cv}}$ ($T_a \ll \tau_{\mathrm{cv}}$) one will obtain a near instantaneous (short-term average) velocity profile $v(z')$ and a small-variance characteristic function $\gamma(z', 2\omega_0\theta/c)$ resulting from the averaged feeble velocity fluctuations whose correlation scales are less than $T_{\mathrm{a}}$.

At $\theta = 0$ from Eq. (1) we obtain the following expression of the mean signal power profile $P(t = 2z/c) = \langle |I(t = 2z/c)|^2 \rangle$:

$$P(t = 2z/c) = \int_{z_0}^{ct/2} f(t - 2z'/c)\Phi(z')\,\mathrm{d}z', \tag{2}$$

where $f(\vartheta) = \langle f_0^2(\vartheta) \rangle = f_\mathrm{m}^2(\vartheta)\eta(\vartheta, \theta = 0) = P_\mathrm{imp}(\vartheta)/P_\mathrm{p}$ is a dimensionless shape describing the mean pulse power shape $P_\mathrm{imp}(\vartheta)$ normalized to its peak value $P_\mathrm{p}$. At known (experimentally determined) $P(t)$ and $f(\vartheta)$, the profile of $\Phi(z')$ can be recovered on the basis of Eq. (2) by using deconvolution techniques [26]. Eq. (2) reveals the sense of $\Phi(z')$ as the contribution to the mean signal power of unitary "scattering length" along the line of sight. When the pulse length is much less than the least variation scale of $\Phi(z')$, instead of Eq. (2) we obtain that $P(t = 2z/c) \cong P_\mathrm{sh}(t = 2z/c) = (c\tau_\mathrm{p}/2)\Phi(z = ct/2)$ where $\tau_\mathrm{p} = \int_0^\infty f(\vartheta)\,\mathrm{d}\vartheta$ is an effective pulse duration, and $l_\mathrm{p} = c\tau_\mathrm{p}$ is the corresponding effective pulse length. The profile of $P_\mathrm{sh}(t = 2z/c)$ [that is obviously proportional to $\Phi(z)$] is mentioned after Eq. (1), for brevity, as the "mean short-pulse ($\delta$-pulse) signal power profile" because it is obtainable at short-enough ($\delta$-like) laser pulses.

We shall consider in this work "exponentially shaped" sensing laser pulses whose mean shape $f_\mathrm{m}(\vartheta)$ is given by

$$f_\mathrm{m}(\vartheta) = \langle f_0(\vartheta) \rangle = (e\vartheta/\tau)\exp(-\vartheta/\tau), \tag{3}$$

where $\tau$ is a time constant determining the pulse duration. We shall also suppose that the relative pulse-shape fluctuations $g(\vartheta)$ are stationary so that the integrand factor $\eta(\vartheta, \theta)$ in Eq. (1) depends only on $\theta$, i.e., $\eta(\vartheta, \theta) \equiv \eta(\theta)$ [$\mathrm{Cov}_\mathrm{g}(\vartheta, \theta) \equiv \mathrm{Cov}_\mathrm{g}(\theta)$]. In addition, since $v(z) \ll c$ and $\delta\omega_\mathrm{ch} \ll \omega_0$, we can assume that the factor $\chi(z')$ explicitly present in Eq. (1) is equal to unity. Under the above conditions and the assumption that the frequency chirp is negligibly small, on the basis of Eq. (1) we have obtained in [10] two algorithms for retrieving the profile of $\omega_\mathrm{m}(z = ct/2)$ [and, respectively, $v(z = ct/2)$] with a resolution cell that can be theoretically of the order of the spatial (temporal) sampling interval $\Delta z$ ($\Delta t = 2\Delta z/c$). The procedure of deriving the retrieval algorithms begins with differentiating Eq. (1) with respect to $t$, includes two more successive differentiations (with respect to $t$ again) and some algebraic transformations, and leads as a final result to an expression of the function

$$\Gamma(t, \theta) = \mathrm{Cov}_{ttt}^{\mathrm{III}}(t, \theta) + (6/\tau)\mathrm{Cov}_{tt}^{\mathrm{II}}(t, \theta) + (12/\tau^2)\mathrm{Cov}_{t}^{\mathrm{I}}(t, \theta) + (8/\tau^3)\mathrm{Cov}(t, \theta), \tag{4}$$

where the symbol "$\overset{\mathrm{I}}{t}$" denotes differentiation with respect to $t$. The expression obtained of $\Gamma(t, \theta)$ [10] leads in turn to the desired algorithms. The first one is given by the relation

$$\omega_\mathrm{m}(z = ct/2) = \theta^{-1}\arctan\{\mathrm{Im}\,\Gamma(t, \theta)/\mathrm{Re}\,\Gamma(t, \theta)\} \tag{5}$$

and is valid when

$$(\omega_\mathrm{m})_t^{\mathrm{I}}\theta^2/2 \ll 1. \tag{6}$$

The second algorithm is given by the relation

$$\omega_\mathrm{m}(z = ct/2) = [\mathrm{Im}\,G(t)]/\{\Phi(z = ct/2)[ce^2\eta(0)/\tau^2]\}, \tag{7}$$

where $G(t) = \Gamma_\theta^{\mathrm{I}}(t, \theta = 0)$ is the first derivative of the function $\Gamma(t, \theta)$ with respect to $\theta$ at $\theta = 0$.

## 3. Retrieving high-resolution Doppler-velocity profiles, taking into account the frequency chirp

On the basis of an analysis of Eq. (1) we shall derive in this section some more general algorithms for retrieving high-resolution Doppler-velocity profiles, taking into account the frequency chirp in the sensing laser pulses. That is, the phase term $\delta\omega_\mathrm{ch}[(t - 2z'/c)\chi(z')]\theta\chi(z') \cong \delta\omega_\mathrm{ch}(t - 2z'/c)\theta$ in Eq. (1) will not be

neglected, and the frequency deviation $\delta\omega_{\rm ch}(\vartheta)$ will be considered as a known function of $\vartheta$ determined experimentally [11–15] or predicted theoretically [13,14]. The characteristic functions $\zeta$, $\xi$, and $\gamma$ in Eq. (1) will be considered as real quantities corresponding to symmetric probability density distributions. We shall also assume that the mean shape of the sensing pulses is given by Eq. (3), and the relative pulse-shape fluctuations $g(\vartheta)$ are stationary, i.e., $\eta(\vartheta,\theta)\equiv\eta(\theta)$ in Eq. (1).

### 3.1. Linear frequency chirp

Let us first show that Eqs. (5) and (7) [together with Eq. (4)] are easy adaptable to the particular case of a linear frequency chirp. The regular frequency deviation $\delta\omega_{\rm ch}(\vartheta)$ in this case is a linear function of $\vartheta$, i.e.,

$$\delta\omega_{\rm ch}(\vartheta)=\omega_{\rm ch}+a\vartheta, \tag{8}$$

where $\omega_{\rm ch}$ is a constant frequency term, and $a[\text{seconds}^{-2}]$ is a constant chirp rate. The term $\omega_{\rm ch}$ leads obviously [see Eq. (1)] to a shift ($=\omega_{\rm ch}$) in the final result for $\omega_{\rm m}(z)$ that can easily be corrected for. Therefore we shall further suppose that $\omega_{\rm ch}=0$ and consider only the modifications in relations (5) and (7) due to the term $a\vartheta$. For a linear frequency chirp $\delta\omega_{\rm ch}(\vartheta)=a\vartheta$ and exponentially shaped laser pulses [Eq. (3)] the integrand factor $f_{\rm m}(t-2z'/c)f_{\rm m}(t+\theta-2z'/c)\exp\{{\rm i}\,\delta\omega_{\rm ch}(t-2z'/c)\theta\}$ in Eq. (1) [$\chi(z')=1$] is equal to $(e/\tau)^2\exp(-\theta/\tau)(t-2z'/c)(t+\theta-2z'/c)\exp\{-Q(t-2z'/c)\}$, where $Q=2/\tau-{\rm j}a\theta$. Thus, the last concrete (explicit) form of the factor considered, as well as the whole Eq. (1), just corresponds to the case of no chirp, where only the quantity $2/\tau$ multiplying $(t-2z'/c)$ in the integrand exponent is formally replaced by $Q$. Then the high resolution profile of $\omega_{\rm m}(z)$ [$v(z)$] can be retrieved again by using Eqs. (5) and (7), where only function $\Gamma(t,\theta)$ should be modified as

$$\Gamma(t,\theta)={\rm Cov}^{\rm III}_{ttt}(t,\theta)+3Q{\rm Cov}^{\rm II}_{tt}(t,\theta)+3Q^2{\rm Cov}^{\rm I}_{t}(t,\theta)+Q^3{\rm Cov}(t,\theta). \tag{4$'$}$$

Let us also note that the additional condition $a\theta^2/2\ll 1$ should be satisfied for Eq. (5) to be valid. This condition is due to the above-indicated substitution $2/\tau\to 2/\tau-{\rm i}a\theta$.

### 3.2. Arbitrary frequency chirp

As a main task to be solved, we shall derive a general retrieval algorithm that is valid for an arbitrary frequency chirp. Under the above-described (Section 3) conditions, on the basis of Eq. (1) we obtain the following expression of the first derivative of ${\rm Cov}(t,\theta)$ with respect to $t$:

$${\rm Cov}^{\rm I}_{t}(t,\theta)=K(\theta)(J_1+J_2)-(2/\tau){\rm Cov}(t,\theta), \tag{9}$$

where

$$K(\theta)=(e/\tau)^2\exp(-\theta/\tau)\zeta(\theta)\xi(\theta)\eta(\theta),$$

$$J_1=\int_0^{ct/2}{\rm d}z'\varphi_1(t,\theta,z')E(t,\theta,z')\Phi(z')\gamma(z',2\omega_0\theta/c),$$

$$J_2={\rm i}\theta\int_{z_0}^{ct/2}{\rm d}z'\varphi_2(t,\theta,z')E(t,\theta,z')\Phi(z')\gamma(z',2\omega_0\theta/c)[\delta\omega_{\rm ch}(t-2z'/c)]^{\rm I}_t,$$

$$\varphi_1(t,\theta,z')=2t-4z'/c+\theta,$$

$$\varphi_2(t,\theta,z')=(t-2z'/c)(t+\theta-2z'/c),$$

$$E(t,\theta,z') = \exp\{-2(t-2z'/c)/\tau + \mathrm{i}[\omega_{\mathrm{m}}(z') + \delta\omega_{\mathrm{ch}}(t-2z'/c)]\theta\}.$$

From Eq. (9), after relocating the term $(2/\tau)\mathrm{Cov}(t,\theta)$ and differentiation with respect to $t$, we obtain the relation

$$\mathrm{Cov}_{tt}^{\mathrm{II}}(t,\theta) + (2/\tau)\mathrm{Cov}_{t}^{\mathrm{I}}(t,\theta) = Y(t,\theta) + K(\theta)(J_3+J_4+J_5) - (2/\tau)[\mathrm{Cov}_{t}^{\mathrm{I}}(t,\theta) + (2/\tau)\mathrm{Cov}(t,\theta)], \quad (10)$$

where

$$Y(t,\theta) = (c\theta/2)K(\theta)\Phi(ct/2)\gamma(ct/2, 2\omega_0\theta/c)\exp\{\mathrm{i}\theta[\omega_{\mathrm{m}}(ct/2) + \delta\omega_{\mathrm{ch}}(0)]\},$$

$$J_3 = 2\int_{z_0}^{ct/2} \mathrm{d}z' E(t,\theta,z')\Phi(z')\gamma(z', 2\omega_0\theta/c),$$

$$J_4 = 2\mathrm{i}\theta\int_{0}^{ct/2} \mathrm{d}z' \varphi_1(t,\theta,z')E(t,\theta,z')\Phi(z')\gamma(z', 2\omega_0\theta/c)[\delta\omega_{\mathrm{ch}}(t-2z'/c)]_t^{\mathrm{I}},$$

$$J_5 = \mathrm{i}\theta\int_{z_0}^{ct/2} \mathrm{d}z' \varphi_2(t,\theta,z')E(t,\theta,z')\Phi(z')\gamma(z', 2\omega_0\theta/c)\varphi_3(t,\theta,z'),$$

$$\varphi_3(t,\theta,z') = [\delta\omega_{\mathrm{ch}}(t-2z'/c)]_{tt}^{\mathrm{II}} + \mathrm{i}\theta\{[\delta\omega_{\mathrm{ch}}(t-2z'/c)]_t^{\mathrm{I}}\}^2.$$

Further we move the term $(2/\tau)[\mathrm{Cov}_t^{\mathrm{I}}(t,\theta) + (2/\tau)\mathrm{Cov}(t,\theta)]$ into the left-hand side of Eq. (10) and differentiate with respect to $t$ again. Thus, we obtain

$$\begin{aligned}\mathrm{Cov}_{ttt}^{\mathrm{III}}(t,\theta) + (4/\tau)\mathrm{Cov}_{tt}^{\mathrm{II}}(t,\theta) + (4/\tau^2)\mathrm{Cov}_{t}^{\mathrm{I}}(t,\theta) &= Y_t^{\mathrm{I}}(t,\theta) + (2/\theta)[1+\theta/\tau + \mathrm{i}\theta^2\delta\omega_{\mathrm{ch}}^{\mathrm{I}}(t-2z'/c=0)] \\ &\quad\times Y(t,\theta) + K(\theta)(J_6+J_7+J_8) - (2/\tau) \\ &\quad\times [\mathrm{Cov}_{tt}^{\mathrm{II}}(t,\theta) + (4/\tau)\mathrm{Cov}_{t}^{\mathrm{I}}(t,\theta) + (4/\tau^2)\mathrm{Cov}(t,\theta)],\end{aligned}$$

that is,

$$\begin{aligned}\Gamma(t,\theta) &= \mathrm{Cov}_{ttt}^{\mathrm{III}}(t,\theta) + (6/\tau)\mathrm{Cov}_{tt}^{\mathrm{II}}(t,\theta) + (12/\tau^2)\mathrm{Cov}_{t}^{\mathrm{I}}(t,\theta) + (8/\tau^3)\mathrm{Cov}(t,\theta) \\ &= Y_t^{\mathrm{I}}(t,\theta) + (2/\theta)[1+\theta/\tau + \mathrm{i}\theta^2\delta\omega_{\mathrm{ch}}^{\mathrm{I}}(t-2z'/c=0)]Y(t,\theta) + K(\theta)(J_6+J_7+J_8),\end{aligned} \quad (11)$$

where

$$J_6 = 6\mathrm{i}\theta\int_{z_0}^{ct/2} \mathrm{d}z' E(t,\theta,z')\Phi(z')\gamma(z', 2\omega_0\theta/c)[\delta\omega_{\mathrm{ch}}(t-2z'/c)]_t^{\mathrm{I}},$$

$$J_7 = 3\mathrm{i}\theta\int_{z_0}^{ct/2} \mathrm{d}z' \varphi_1(t,\theta,z')E(t,\theta,z')\Phi(z')\gamma(z', 2\omega_0\theta/c)\varphi_3(t,\theta,z'),$$

$$J_8 = \mathrm{i}\theta\int_{z_0}^{ct/2} \mathrm{d}z' \varphi_2(t,\theta,z')E(t,\theta,z')\Phi(z')\gamma(z', 2\omega_0\theta/c)\varphi_4(t,\theta,z'),$$

$$\varphi_4(t,\theta,z') = 3\mathrm{i}\theta[\delta\omega_{\mathrm{ch}}(t-2z'/c)]_t^{\mathrm{I}}[\delta\omega_{\mathrm{ch}}(t-2z'/c)]_{tt}^{\mathrm{II}} + [\delta\omega_{ch}(t-2z'/c)]_{ttt}^{\mathrm{III}} - \theta^2\{[\delta\omega_{\mathrm{ch}}(t-2z'/c)]_t^{\mathrm{I}}\}^3,$$

and $\delta\omega_{\mathrm{ch}}^{\mathrm{I}}(t-2z'/c=0)$ is the derivative $[\delta\omega_{\mathrm{ch}}(t-2z'/c)]_t^{\mathrm{I}}$ at $z'=ct/2$.

On the basis of Eq. (11) we obtain the following expression of the imaginary part of the first derivative $G(t) = \Gamma^{\mathrm{I}}_{\theta}(t, \theta = 0)$ of the function $\Gamma(t, \theta)$ with respect to $\theta$ at $\theta = 0$:

$$\mathrm{Im}\, G(t) = (ce^2/\tau^2)\eta(0)\Phi(z = ct/2)[\omega_{\mathrm{m}}(z = ct/2) + \delta\omega_{\mathrm{ch}}(0)] + R(t), \tag{12}$$

where

$$R(t) = (e/\tau)^2\eta(0)\int_{z_0}^{ct/2} \mathrm{d}z'[(t - 2z'/c)^2\delta\omega_{\mathrm{ch}}(t - 2z'/c)]^{\mathrm{III}}_{ttt} \exp[-2(t - 2z'/c)/\tau]\Phi(z').$$

In turn, Eq. (12) leads to the relation

$$\omega_{\mathrm{m}}(z = ct/2) = [\mathrm{Im}\, G(t) - R(t)]/\{\Phi(z = ct/2)[ce^2\eta(0)/\tau^2]\} - \delta\omega_{\mathrm{ch}}(0), \tag{13}$$

which is a general algorithm we had to develop for retrieving the mean Doppler-velocity profile $v(z = ct/2)$ $[\omega_{\mathrm{m}}(z = ct/2)]$ with a resolution interval of the order of $\Delta z$ ($\Delta t$). The algorithm obtained [Eq. (13)] differs formally from Eq. (7) in the appearance of the terms $R(t)$ and $\delta\omega_{\mathrm{ch}}(0)$ accounting for the frequency chirp $\delta\omega_{\mathrm{ch}}(\vartheta)$ considered as arbitrary in form but differentiable function of $\vartheta$.

## 4. Simulations

In this section we represent some results from simulations we have conducted to investigate and illustrate to what extent it is important to take into account the frequency chirp in the sensing laser pulses by using the developed above inverse techniques (algorithms) for retrieving high-resolution Doppler-velocity profiles. The wavelength of the sensing radiation $\lambda = 2\pi c/\omega_0$ is supposed to be $\lambda = 10.6$ μm ($CO_2$ lidars) or $\lambda = 2$ μm (solid-state lidars). The case of a stable reproducible pulse shape is considered, when $g(\vartheta) \equiv 0$, and $f(\vartheta) = f_0^2(\vartheta) = (e^2\vartheta^2/\tau^2)\exp(-2\vartheta/\tau)$.

The realizations of the complex heterodyne signal $I(t) = J(t) + \mathrm{i}Q(t)$ are simulated (as in [9,10,27]) by taking into account the fact that because of the incoherent character of the aerosol backscattering process the polarization components of the backscattered radiation can be considered as circular complex Gaussian random quantities. Since our purpose is to reveal mainly the chirp influence on the algorithm performance, we have not simulated random frequency ($\delta\omega_{\mathrm{r}}$) and phase ($\varphi_{\mathrm{r}}$) fluctuations and random radial-velocity fluctuations $\tilde{v}(z)$. In other words, the case is implied when the effect of the frequency chirp is more essential than the effect of the random phase fluctuations. We have not simulated either additive random noise. The influence of these (above-mentioned) random factors on the accuracy of the retrieved Doppler-velocity profiles is investigated by simulations in [10]. In the present work only the speckle noise is naturally present. This means that the actual single-shot signal-to-noise ratio (SNR) is equal to unity [28–31]. The situation is nearly the same (SNR $<\approx 1$) when the signal power exceeds the power of the shot noise and other additive noise, that is, when the additive noise exists, but the speckle noise is prevailing. The contemporary high pulse repetition rate laser transmitters (some of them cited below) for coherent lidars are designed in such a way that to ensure powerful enough signals, in the above sense, from distances of several kilometers within the planetary boundary layer. To enlarge the effective SNR one should certainly use some averaging and filtering procedures.

The covariance estimates are obtained according to the relation

$$\widehat{\mathrm{Cov}}(t, \theta = m\Delta t) = N^{-1}\sum_{k=1}^{N} I_k^*(t)I_k(t + m\Delta t), \tag{14}$$

where $t = l\Delta t = 2l\Delta z/c$ ($l = 0, 1, 2, \ldots$), and $N$ is the number of realizations employed $I_k(t)$. At $m = 0$, Eq. (14) provides the estimate $\hat{P}(t) = \widehat{\mathrm{Cov}}(t, \theta = 0)$ of the signal power profile $P(t) = \mathrm{Cov}(t, \theta = 0)$. After $\hat{P}(t)$ is

known, we obtain by deconvolution [26], on the basis of Eq. (2), the estimate $\hat{\Phi}(z = ct/2)$ of the short-pulse signal power profile $\Phi(z = ct/2)$.

At an arbitrary high number of signal realizations ($N \to \infty$), under stationary conditions, the random error (caused by various random factors) in the restored Doppler-velocity profiles will be negligibly small. If, in addition, some possible bias errors are also compensated for (see, e.g. [10]), one would achieve accurately restored profiles with a range resolution cell $\rho$ that is of the order of the sampling (and data processing) interval $\Delta z$. However, even if high pulse repetition rate lasers are used [see, e.g. [11] and [12]), an enormously high value of $N$ would require a too long data accumulation time exceeding the period of stationarity of the atmospheric conditions. Therefore, some type of filtering is necessary to suppress the effect of the random factors and thus to ensure a satisfactory quality of the restored profiles at a reasonable number $N$ of signal realizations (respectively, laser pulses, laser shots). However, the filtering procedure lowers the range resolution. As it is shown in Appendix A, the resolution cell $\rho$ will be already of the order of the width $W$ of the window of the filter employed. To retain a satisfactory range resolution the value of $W$ should be less than the least variation scale (along the line of sight) $\Lambda_v$ of the mean radial velocity $v(z)$. Then the restored velocity profiles $v_r(z)$ are minimally distorted with respect to the true ones, $v(z)$. In this case the variability of $\Phi(z)$, reflecting the backscatter gradients along the line of sight, has no influence on the retrieval resolution. When $W$ exceeds $\Lambda_v$ the small-scale velocity variations (whose scales are less than $W$) will be unresolved or strongly distorted in the restored profiles. The small-scale velocity variations may be additionally distorted because of strong local backscatter gradients whose scales $\Lambda_\Phi$ are less than $W$. We have used for the simulations a smooth monotone sharp-cutoff digital filter [32] with $\pi/(9\Delta t)$-wide passband for smoothing the estimates $\widehat{\mathrm{Cov}}(t, \theta)$, $\widehat{\mathrm{Cov}}(t, 0)$, $\hat{\Phi}(z = ct/2)$, and the restored profiles $v_r(z = ct/2)$. The corresponding range resolution cell is $\rho \sim W = 9c\Delta t/2 = 9\Delta z$ (in the range domain).

### 4.1. Chirp effect in $CO_2$ lidars

As we mentioned in Section 1, the chirp effect in $CO_2$ lidars ($\lambda = 10.6$ μm) is more important than in solid-state lidars ($\lambda = 2$ μm). Therefore we shall begin with (and mainly investigate) the case of $CO_2$ lidars. The model of the mean Doppler-velocity profile $v(z)$ considered in this case is shown in Fig. 1(a). It is chosen to be like a sequence of wind vortices having relatively small spatial size and sharp velocity variations; the velocity variations scale $\Lambda_v$ is about 150 m. The backscattering variability is modelled through the profile of $\Phi(z)$ that is given in Fig. 1(b); the variation scale $\Lambda_\Phi$ of the profile $\Phi(z)$ is about 75 m. The pulse power shape $f(\vartheta)$ employed in the simulations is shown in Fig. 2 (solid curve). The value of $\tau$ is

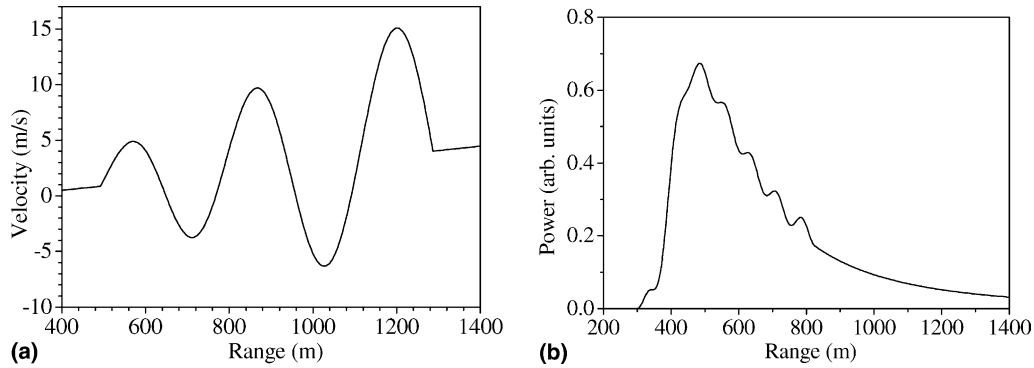


Fig. 1. Models of (a) the mean Doppler-velocity profile $v(z)$ and (b) the mean short-pulse signal power profile $\Phi(z)$ used in the simulations for $\lambda = 10.6$ μm.

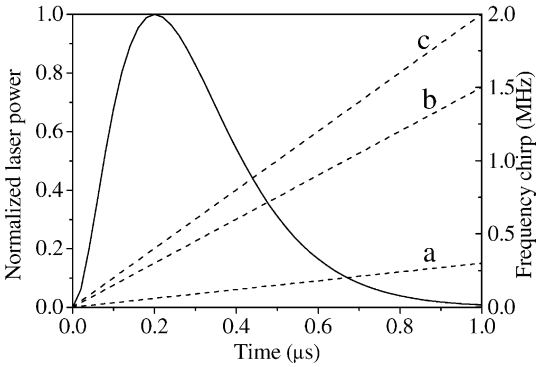


Fig. 2. Models of the pulse power shape for $\tau = 200$ ns (solid curve) and the linear frequency chirp (dashed lines) with rates $a_1 = 0.3$ MHz/μs (a), 1.5 MHz/μs (b), and 2 MHz/μs (c).

supposed to be 200 ns that corresponds to a pulse length $l_p \sim 300$ m (pulse duration $\tau_p \sim 1$ μs), which exceeds the variation scales $\Lambda_v$ and $\Lambda_\Phi$. The sampling interval $\Delta t = 2\Delta z/c$ and the lidar blind zone upper limit $z_0$ are chosen to be, respectively, $\Delta t = 20$ ns ($\Delta z = 3$ m) and $z_0 = 300$ m.

Let us first consider the results from simulating the algorithm performance in the case of an increasing linear frequency chirp $\delta\omega_{ch}(\vartheta) = a\vartheta = 2\pi a_1\vartheta$ whose rate $a(a_1)$ may have various values (Fig. 2, dashed lines). The number of simulated signal realizations is $N = 300$, and a smoothing of $\widehat{\mathrm{Cov}}(t,\theta)$, $\widehat{\mathrm{Cov}}(t,0)$, $\hat{\Phi}(z = ct/2)$, and $v_r(z = ct/2)$ is performed, as it is explained above, by use of a smooth monotone sharp-cutoff digital filter [32] with $9\Delta z$-wide window. Thus, a resolution cell $\rho \sim 27$ m is achieved that is much less than the resolution cell $\rho_p = l_p/2$ (~150 m) defined by the pulse length $l_p \sim 300$ m. (Let us note meanwhile that a resolution cell of the order of $\rho_p$ does not allow one to avoid sensible distortions when retrieving (e.g., by use of pulse pair algorithm) velocity profile features having sizes of the same order or shorter.) The value of $\rho$ is also much less than $\Lambda_v$ and $\Lambda_\Phi$. When the frequency chirp is taken into account and we use Eq. (13) or Eqs. (5) or (7) [with $\Gamma(t,\theta)$ given by Eq. (4′)] for retrieving $v(z)$, there is no noticeable bias error in the determination of $v_r(z)$ by simulations (see Fig. 3, solid curves). That is, the recovered Doppler-velocity profiles $v_r(z)$ practically coincide with the original model $v(z)$. When algorithms (5) and (7) are employed without any correction for the chirp [$\Gamma(t,\theta)$ is given by Eq. (4)], there arises a bias error $\delta v_r(z) = v_r(z) - v(z)$ in the

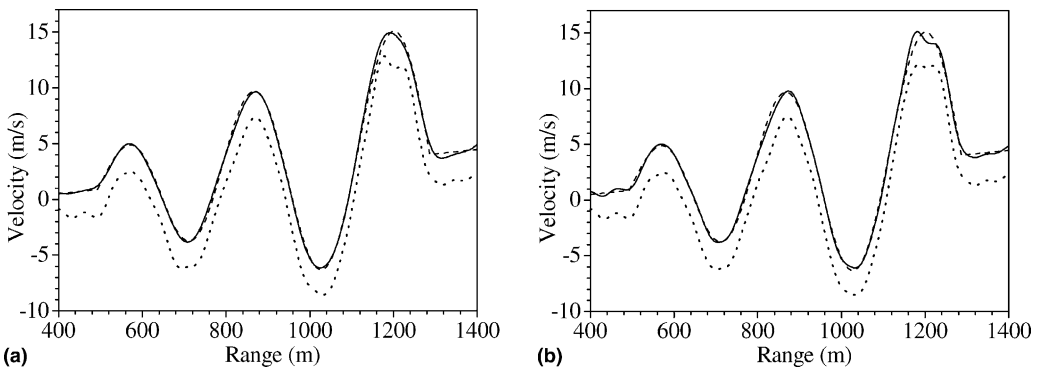


Fig. 3. Doppler-velocity profiles $v_r(z)$ restored by use of (a) algorithm (5) and (b) algorithm (7) with (solid curves) and without (dotted curves) correction for the chirp in the case of increasing linear chirp with rate $a_1 = 1.5$ MHz/μs. The original profile $v(z)$ (dashed curve) is given for comparison; $\lambda = 10.6$ μm.

determination of the Doppler-velocity profiles $v_r(z)$ that is noticeable for $a_1 > 0.3$ MHz/μs. This error increases with the increase of the chirp rate $a_1$ and has the same (certainly negative) sign at every distance $z$ along the line of sight (see Fig. 3, dotted curves). In Fig. 4 we have represented the behaviour of the mean bias error $\delta v_r = \int_{z_1}^{z_2} dz \delta v_r(z)/(z_2 - z_1)$, evaluated on the basis of results from simulations, as a function of the chirp rate $a_1$. The value of $\delta v_r$ is obtained by averaging $\delta v_r(z)$ over the range of the Doppler-velocity profile under consideration, from $z = z_1 = 480$ m to $z = z_2 = 1300$ m. It is seen that when the chirp is accounted for, there is no practically chirp-due error for all considered values of the chirp rate $a_1$. In the case of no chirp correction the module of the error $|\delta v_r|$ increases linearly with $a_1$. The dependence of $\delta v_r$ on $a_1$ can also be evaluated independently (before simulations), taking into account that according to Eq. (13) the intermediate frequency bias $\delta\omega_m(z) = R(t = 2z/c)/\{\Phi(z)[ce^2\eta(0)/\tau^2]\} + \delta\omega_{ch}(0)$. It is seen in Fig. 4 that the latter "theoretical" dependence given by solid line is in accordance with the one obtained by simulations.

Further we have simulated the algorithm performance for a more complicated behaviour of the frequency deviation $\delta\omega_{ch}(\vartheta) = 2\pi\delta\nu_{ch}(\vartheta)$ in the sensing laser pulse. Function $\delta\nu_{ch}(\vartheta)$ is represented graphically in Figs. 5(a)–(c) (insets), where it is seen to retain its form but to progressively lower its minimum. Such a chirp form is like the one intrinsic to the TEA-$CO_2$ laser pulses [13,14], but can be considered as arbitrarily chosen in all other respects. The simulations of the retrieving procedure without any correction for the chirp [by use of Eqs. (5) and (7) together with Eq. (4)] ascertain the appearance of a positive bias error in the determination of the Doppler-velocity profiles (see Fig. 5) that corresponds to the wholly negative

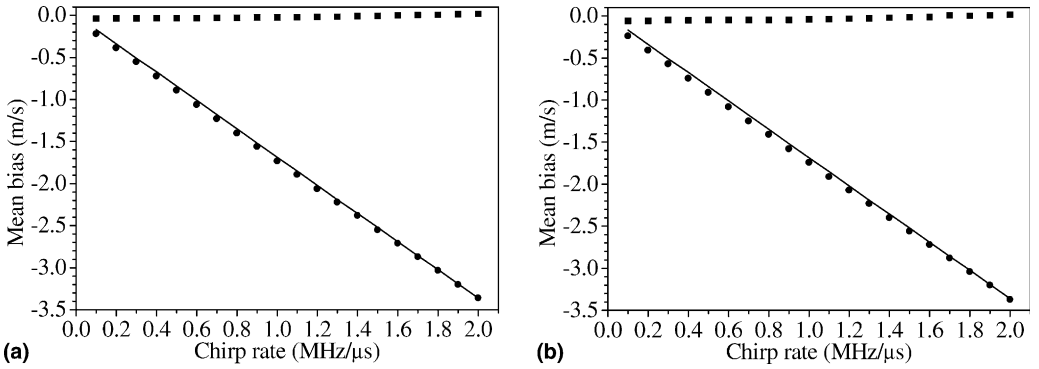


Fig. 4. Mean bias error in the determination of $v_r(z)$ [restored by use of (a) algorithm (5) and (b) algorithm (7) without (circles) and with (squares) chirp correction] as a function of chirp rate in the case of increasing linear frequency chirp; $\lambda = 10.6$ μm. The independently evaluated mean bias error is given for comparison by solid curve.

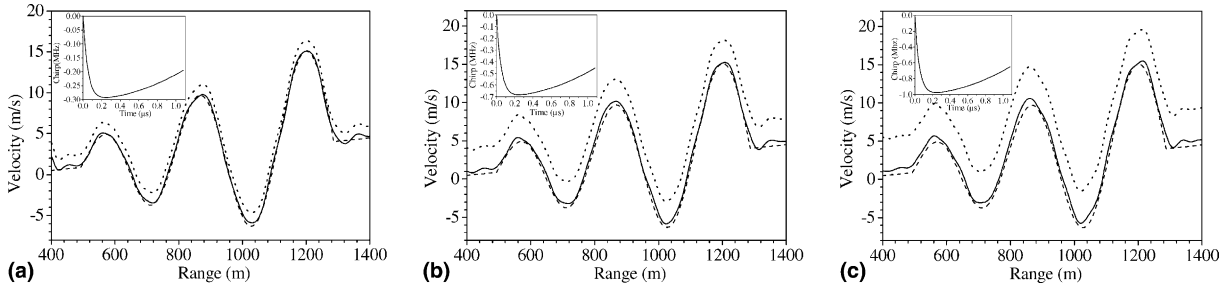


Fig. 5. Doppler-velocity profiles $v_r(z)$ restored by use of algorithm (13) (solid curves) and algorithm (7) (dotted curves) in the case of the frequency chirp given in insets, with chirp module maximum 0.3 MHz (a), 0.7 MHz (b), and 1 MHz (c). The original profile $v(z)$ (dashed curve) is given for comparison; $\lambda = 10.6$ μm.

frequency chirp. The bias error becomes noticeable when the module of the maximum (negative) chirp deviation exceeds 0.1 MHz, i.e., when the minimum of function $\delta v_{ch}(\vartheta)$ is below −0.1 MHz. The mean error $\delta v_r$ in this case increases again linearly considered as a function of the chirp module maximum (Fig. 6, circles). The theoretical dependence evaluated independently on the basis of the expression of $\delta\omega_m(z)$ (see Fig. 6, solid curve) has a similar behaviour. The simulations of the retrieving procedure based on Eq. (13), that takes into account the frequency chirp, show that in this case the Doppler-velocity profiles are accurately restored (see Figs. 5 and 6). Since the same number $N$ of signal realizations and the same filtering as above are employed the resolution cell achieved $\rho$ is again of the order of 27 m.

The observation (data accumulation) time, which is necessary for accumulation of $N$ realizations ensuring an accurate retrieving of the Doppler-velocity profiles depends on the pulse repetition rate of the laser transmitters employed. At a sufficiently high pulse repetition rate the observation time can be of the order of seconds, which is an acceptable value in regard to the stationarity of the atmospheric conditions. For instance, a $CO_2$ laser with 300 Hz pulse repetition rate [11] allows one to accumulate $N = 300$ signal realizations for only one second. It is just the case considered in this subsection where the pulse duration (pulse length) assumed is $\tau_p = 1$ μs ($l_p = 300$m). For longer sensing pulses the speckle-noise influence on the algorithm performance is stronger [33] and the number $N$ required of laser pulses is larger. So for 3–4 μs long laser pulses a number of 1000–2000 pulses (realizations) is necessary to retrieve satisfactorily the Doppler-velocity profiles. The corresponding data accumulation time (for 300 Hz pulse repetition rate) is ~3.3–6.7 s. For a pulse repetition rate of 1000 Hz (see, e.g. [34,35]) the observation time is already ~1–2 s.

To illustrate the above-discussed conception (rather than definition) of the range resolution as conditioned by the width $W$ of the filter window, we have performed some additional simulations where we have introduced a new model of $\Phi(z)$ (reflecting the line-of-sight backscatter distribution) and a new model of the mean radial velocity profile $v(z)$. They are represented, respectively, in Fig. 7(a) (dotted curve) and Fig. 7(b) (dashed curve). The chirp form assumed is given in Fig. 7(b) (inset). The new profile of $\Phi(z)$ involves some strong inhomogeneities (strong backscatter gradients) whose scales are less than $W$ (~27 m). The new velocity profile contains a sequence of oscillations whose period decreases with the range along the line of sight. At the same time the oscillation amplitude increases with the range. We have first simulated the case when the model of $\Phi(z)$ having strong inhomogeneities is combined with the former relatively slowly varying model of $v(z)$. The restored velocity profile in this case, $v_r(z)$, is compared in Fig. 7(a) with $v(z)$. It is seen that the two profiles, $v_r(z)$ and $v(z)$, are closely coincident, independently of the presence of strong backscatter gradients. That is (see Appendix A), filtering leads only to replacing $\Phi(z)$ [in Eq. (1), and,

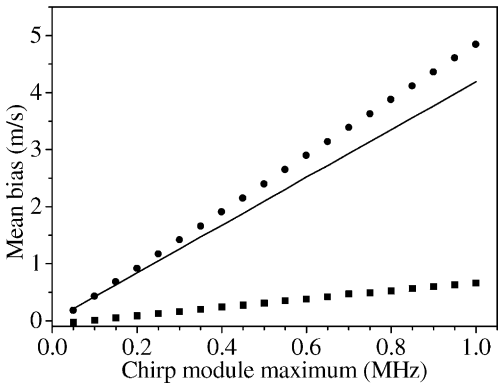


Fig. 6. Mean bias error in the determination of $v_r(z)$ [restored by use of algorithm (13) (squares) and algorithm (7) (circles)] as a function of chirp module maximum in the case of the frequency chirp form represented in Fig. 5. The independently evaluated mean bias error is given for comparison by solid curve.

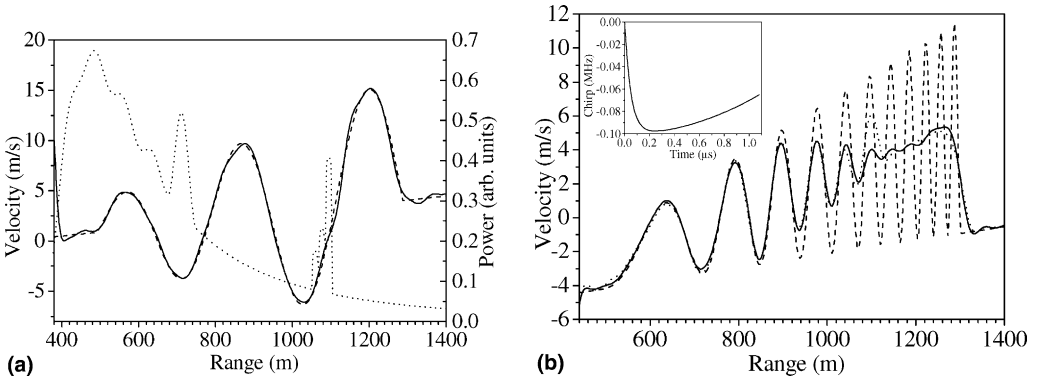


Fig. 7. Doppler-velocity profiles $v_r(z)$ restored by use of algorithm (13) and compared with the original profiles $v(z)$ (dashed curves) in the case of (a) slow velocity and sharp backscatter variations and (b) sharp velocity variations combined with slow (solid curve) and sharp (dotted curve) backscatter variations at a range-resolution cell $\rho \sim 27$ m; $\lambda = 10.6$ μm.

respectively, in Eq. (13)] with a smoothed profile $\Phi_{sm}(z)$ without sensible changes in $v(z)$. Further we have simulated the case where the fast-varying model of $v(z)$ is combined with the former relatively smooth model of $\Phi(z)$ (Fig. 1(b)). In this case, as it is seen in Fig. 7(b) (solid curve), the first velocity variations, whose scale exceeds the filter window $W$, are accurately recovered. The following variations, whose scale is comparable with $W$, are already apparently distorted, especially in their sharply varying (extremum) parts. The final variations, whose scale is less than $W$, are unresolved. Similar results (Fig. 7(b), dotted curve) are obtained from the final simulations where the profiles assumed of $\Phi(z)$ and $v(z)$ have fast variable features. The large-scale velocity variations (at near distances along the line of sight) are again accurately recovered despite of the presence there of sharp backscatter gradients. The small-scale variations (at further distances) are smoothed or unresolved, including some additional distortions around the location of strong backscatter gradients. As a whole, the results from the simulations confirm the conclusion (analytically deduced in Appendix A) that the ability to accurately reconstruct (resolve) the Doppler-velocity profiles is determined mainly by the velocity variability (the velocity gradients) within the filter window.

### 4.2. Chirp effect in solid-state lidars

Although the chirp effect is not so essential for the contemporary solid-state lidars it is briefly considered here for completeness. Besides, it might be important in some future, advantageous in many respects (e.g., powerful, high pulse repetition rate) solid-state laser transmitters. The wavelength of the sensing laser radiation is assumed to be $\lambda = 2$ μm.

The simulations are performed at shorter laser pulses, $\tau$ is 100 ns, and shorter sampling intervals, $\Delta t = 10$ ns ($\Delta z = 1.5$ m), compared with the case of $CO_2$ lidars. Correspondingly, the model of the Doppler-velocity profile (Figs. 8(a) and (b), dashed curves) is shorter to scale. The model of the short-pulse signal power profile [$\propto \Phi(z)$] is the same as above (Fig. 1(b)). The frequency chirp has the same form as for $\lambda = 10.6$ μm but is compressed over a shorter temporal interval corresponding to the shorter laser pulse (see Figs. 8(a) and (b), inset). The number of signal realizations is $N = 200$ and the same filtering as above is performed. Thus, taking into account the shorter sampling interval $\Delta z = 1.5$ m, the resolution cell achieved now is $\rho \sim 13.5$ m, which is much less than $l_p/2$ (~75 m), $\Lambda_v$ (~70 m), and $\Lambda_\Phi$ (~75 m). At a pulse repetition rate of, e.g., 200 Hz [4,6,36–38] the data accumulation time will be equal to 1 s. Let us note that 1 kHz pulse repetition rate is also achievable in the recent 2 μm solid-state lidars (see, e.g. [36–38]). The simulations of the retrieving procedure accounting for the chirp [based on Eq. (13)] show that in this case the Doppler-velocity profiles are accurately recovered (Figs. 8(a) and (b); solid curves). When the chirp is

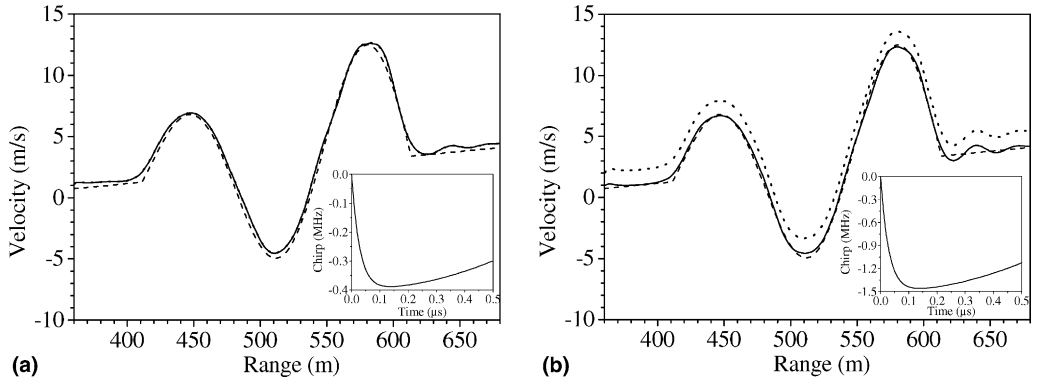


Fig. 8. Doppler-velocity profiles $v_r(z)$ restored by use of algorithm (13) (solid curves) and algorithm (7) (dotted curves) in the case of the frequency chirp given in insets with chirp module maximum = 0.4 MHz (a) and 1.5 MHz (b). The original profile $v(z)$ (dashed curve) is given for comparison; $\lambda = 2$ μm.

not corrected for, the above-discussed positive bias arises. Certainly, this bias increases with the increase of the chirp module maximum (see Figs. 8(a) and (b), dotted curves) with a lower rate compared with the case of $\lambda = 10.6$ μm.

As a whole, the simulations conducted show that the algorithms derived in the paper [Eq. (13), and Eqs. (5) and (7) with $\Gamma(t,\theta)$ given by Eq. (4′)] allow one to retrieve accurately the Doppler-velocity profiles in the presence of arbitrary frequency chirp in the sensing laser pulses, with a resolution cell that is much less than the pulse length. Filtering the covariance estimate $\widehat{\mathbf{Cov}}(t,\theta)$ and the retrieved profile $v_r(z)$ [corresponding to $v(z)$], as well as $\hat{P}(t)$ and $\hat{\Phi}(z = ct/2)$, is a way to suppress the noise influence and thus to reduce the number of signal realizations (laser shots) $N$ required to ensure a prescribed accuracy. However, the effective width of the filter window should have an optimum (not very large) value ensuring a satisfactory noise suppression at an acceptable range resolution.

## 5. Conclusion

In the present work we have generalized some inverse mathematical techniques for improving the range resolution of determining Doppler-velocity profiles on the basis of data from coherent heterodyne lidars with exponentially shaped sensing laser pulses. The extended techniques are based on an analysis of the complex heterodyne signal autocovariance and are valid for the general case when an arbitrary frequency chirp is present in the sensing laser pulses. The ideal resolution cell can be in principle of the order of the sampling intervals, at an arbitrary high number $N$ of signal realizations ensuring effective noise suppression. The real achievable resolution cell however is larger because of the necessity of lowering the number $N$ required, by filtering at least the speckle noise effects disturbing the final results. The resolution cell is then of the order of the width of the window of the filters employed, but remains much less than the sensing laser pulse length. The reduced value of $N$ requires a shorter observation (data accumulation) time that can be of the order of seconds when using powerful enough, high pulse repetition rate laser transmitters.

## Acknowledgements

The authors are grateful to Prof. Dimitar Stoyanov for the fruitful and stimulating discussions on the problems concerned in the paper. This research was supported in part by the Bulgarian National Science Fund under Grant F-907.

## Appendix A. Estimating the influence of filtering on the velocity-profile retrieval resolution

For convenience, we shall describe the digital filtering process in the time (or range) domain by an approximative continuous waveform $D(\vartheta)$ such that $D(\vartheta) = D(-\vartheta) > 0$, $\lim_{\vartheta\to\pm\infty} D(\vartheta) = 0$, $D(\vartheta = 0) = D_{\max}$ is the only maximum of $D(\vartheta)$, and $\int_{-\infty}^{\infty} D(\vartheta)\,\mathrm{d}\vartheta = 1$; the dimension of $D(\vartheta)$ is $[time^{-1}]$. The effective width $w$ of the waveform (the filtering function) $D(\vartheta)$ in the time domain can be defined as $w = \int_{-\infty}^{\infty} [D(\vartheta)/D_{\max}]\,\mathrm{d}\vartheta = D_{\max}^{-1}$. The width (window) in the range domain is $W = cw/2 = c/2D_{max}$. As a consequence of filtering, the expression of the signal autocovariance [Eq. (1)] is modified in the following way:

$$\mathrm{Cov}_{\mathrm{m}}(t,\theta) = \int_{-\infty}^{\infty} D(t-t')\mathrm{Cov}(t',\theta)\,\mathrm{d}t', \tag{A.1}$$

where $\mathrm{Cov}(t',\theta)$ is the expression of the autocovariance given by Eq. (1). By using the substitution $t - 2z'/c = x$, taking into account that by definition $f(\vartheta) \equiv 0$ for $\vartheta \leq 0$, and $\Phi(z) \equiv 0$ for $z \leqslant z_0$, Eq. (1) can be rewritten in the form

$$\mathrm{Cov}(t',\theta) = \int_{-\infty}^{\infty} H(x,z\theta)Q(t'-x,\theta)\,\mathrm{d}x, \tag{A.2}$$

where $H(x,\theta) = B(\theta)f_{\mathrm{m}}(x)f_{\mathrm{m}}(x+\theta)\exp\{\mathrm{i}\delta\omega_{\mathrm{ch}}(x)\theta\}$, $B(\theta) = \zeta(\theta)\xi(\theta)\gamma(2\omega_0\theta/c)$, and $Q(t'-x,\theta) = \Phi[c(t'-x)/2]\exp\{\mathrm{i}\omega_{\mathrm{m}}[c(t'-x)/2]\theta\}$. As it is mentioned in Section 2, we suppose that the factor $\chi(z')$ explicitly present in Eq. (1) is equal to unity. Also it is assumed for simplicity that function $\gamma(z', 2\omega_0\theta/c) \equiv \gamma(2\omega_0\theta/c)$, i.e., $\gamma$ does not depend on $z'$ at least within a pulse length. If we use in Eq. (A.1) the expression of $\mathrm{Cov}(t',\theta)$ given by Eq. (A.2) we obtain

$$\mathrm{Cov}_{\mathrm{m}}(t,\theta) = \int_{-\infty}^{\infty} H(x,\theta)Q_{\mathrm{m}}(t-x,\theta)\,\mathrm{d}x, \tag{A.3}$$

where function

$$\begin{aligned} Q_{\mathrm{m}}(t-x,\theta) &= \int_{-\infty}^{\infty} D(t-t')Q(t'-x,\theta)\,\mathrm{d}t' \\ &= \int_{-\infty}^{\infty} D(y)\Phi[c(t-x+y)/2]\exp\{\mathrm{i}\omega_{\mathrm{m}}[c(t-x+y)/2]\theta\}\,\mathrm{d}y \end{aligned} \tag{A.4}$$

describes the effect of filtering. For more viewable analysis of this effect we shall consider the (realistic) case when $2v(z)\omega_0\theta/c \ll 1$. In this case the exponential integrand factor in Eq. (A.4) can be approximated as $\exp[\mathrm{i}(\omega_{\mathrm{m}}(z)\theta] \cong \exp[\mathrm{i}(\omega_0 - \omega_{\mathrm{h}})\theta][1 - \mathrm{i}2v(z)\omega_0\theta/c]$. Then, according to the law of the mean, Eq. (A.4) acquires the form

$$Q_{\mathrm{m}}(t-x,\theta) \cong \Phi_{\mathrm{sm}}[c(t-x)/2]\exp\{\mathrm{i}\omega_{\mathrm{md}}[c(t-x)/2]\theta\}, \tag{A.5}$$

where functions $\Phi_{\mathrm{sm}}[z = c\vartheta/2] = \int_{-\infty}^{\infty} D(y)\Phi[c(\vartheta+y)/2]\,\mathrm{d}y = \Phi[z = c(\vartheta+y_1)/2]$ and $\omega_{\mathrm{md}}(z = c\vartheta/2) = \omega_0 - \omega_{\mathrm{h}} - 2\omega_0 v_d(c\vartheta/2)/c = \omega_0 - \omega_{\mathrm{h}} - 2(\omega_0 v[z = c(\vartheta+y_2)/2]/c$ describe the distorted (smoothed), in general, backscatter and velocity profiles respectively; the quantities $y_1$ and $y_2$ should mostly lie within the interval $[-w/2, w/2]$ and depend on $\vartheta$, that is, on the behaviour of $\Phi(z)$ and $v(z)$ around $z = c\vartheta/2$. The expression of Eq. (A.5) shows [see also Eq. (A.3)] that due to filtering the expression of the autocovariance [Eq. (A.2) or Eq. (1)] is modified in such a way that the smoothed profiles $\Phi_{\mathrm{sm}}(z)$ and $\omega_{\mathrm{md}}(z)$ take the places of the true ones, $\Phi(z)$ and $\omega_{\mathrm{m}}(z)$ respectively. Consequently, the retrieving procedure consists now in determining first $\Phi_{\mathrm{sm}}(z)$ on the basis of Eq. (2) [obtainable from Eq. (1) at $\theta = 0$], and then, in determining $v_d(z)$ on the basis of Eq. (13). Let us note however that along range intervals having no sharp backscatter gradients on the scales $\sim W$, the profiles $\Phi_{\mathrm{sm}}(z)$ and $\Phi(z)$ practically coincide because then $\Phi(z = c\vartheta/2) \cong \Phi[z = c(\vartheta + y_1)/2]$.

This means that the distribution of $\Phi(z)$ along the mentioned range intervals will be accurately recovered, independently of the velocity gradients. Vice versa, along range intervals with slow velocity variations on scales $\sim W$, the velocity profile $v(z)$ will be accurately restored, independently of the backscatter gradients; then $v(z = c\vartheta/2) \cong v[z = c(\vartheta + y_2)/2]$. When there are strong coincident backscatter and velocity gradients along the line of sight, the recovered profiles will be additionally mutually distorted.

The general conclusion is that the possibility to accurately reconstruct the profile $\Phi(z)$ is determined by the backscatter variability (the backscatter gradients) along the line of sight, independently of the velocity gradients. The ability to accurately reconstruct the radial velocity profile $v(z)$ is determined by the velocity gradients along the line of sight, independently of the backscatter gradients.

## References


[1] M.J. Post, R.E. Cupp, Appl. Opt. 29 (1990) 4145.
[2] J.W. Bilbro, C. DiMarzio, D. Fitzjarrald, S. Johnson, W. Jones, Appl. Opt. 25 (1986) 2952.
[3] G.N. Pearson, B.J. Rye, Appl. Opt. 31 (1992) 6475.
[4] R. Targ, B.C. Steakley, J.G. Hawley, L.L. Ames, P. Forney, D. Swanson, R. Stone, R.G. Otto, V. Zarifis, Ph. Brockman, R.S. Calloway, S.H. Klein, P.A. Robinson, Appl. Opt. 35 (1996) 7117.
[5] S.W. Henderson, C.P. Hale, J.R. Magee, M.J. Kavaya, A.V. Huffaker, Opt. Lett. 16 (1991) 773.
[6] V. Wulfmeyer, M. Randall, A. Brewer, R.M. Hardesty, Opt. Lett. 25 (2000) 1228.
[7] R. Frehlich, S.M. Hannon, S.W. Henderson, Appl. Opt. 36 (1997) 3491.
[8] S.M. Hannon, J.A. Thomson, J. Mod. Opt. 41 (1994) 2175.
[9] L.L. Gurdev, T.N. Dreischuh, D.V. Stoyanov, J. Opt. Soc. Am. A 18 (2001) 134.
[10] L.L. Gurdev, T.N. Dreischuh, D.V. Stoyanov, Appl. Opt. 41 (2002) 1741.
[11] J.-L. Lachambre, P. Lavigne, M. Verreault, G. Otis, IEEE J. Quantum Electron. 14 (1978) 170.
[12] P.W. Pace, J.M. Cruickshank, IEEE J. Quantum Electron. 16 (1980) 937.
[13] D.V. Willets, M.R. Harris, J. Phys. D 15 (1982) 51.
[14] D.V. Willets, M.R. Harris, IEEE J. Quantum Electron. 19 (1983) 810.
[15] G. Scott, A.L.S. Smith, Opt. Commun. 50 (1984) 325.
[16] Y.L. Sun, R.L. Byer, Opt. Lett. 7 (1982) 408.
[17] A.M. Dabas, P. Drobinski, P.H. Flamant, J. Atmos. Ocean. Tech. 15 (1998) 407.
[18] K.S. Miller, M.M. Rochwarger, IEEE Trans. Inform. Theory 18 (1972) 588.
[19] D.S. Zrnic, IEEE Trans. Geosci. Electron. 17 (1979) 113.
[20] J.A. Weiss, J.M. Schnur, Appl. Phys. Lett. 22 (1973) 453.
[21] T.J. Kane, J.D. Kmetec, in: Coherent Laser Radar, 1995 OSA Technical Digest Series, vol. 19, Optical Society of America, Washington, DC, 1995, p. 285.
[22] S. Schnell, V. Ostroumov, J. Breguet, W. Luethy, H. Weber, I. Shcherbakov, IEEE J. Quantum Electron. 26 (1990) 1111.
[23] J. Liu, D. Shen, S.-C. Tam, Y.-L. Lam, IEEE J. Quantum Electron. 37 (2001) 888.
[24] J. Dong, P. Deng, Y. Liu, Y. Zhang, J. Xu, W. Chen, X. Xie, Appl. Opt. 40 (2001) 4303.
[25] T. Kondoh, S. Lee, D.P. Hutchinson, R.K. Richards, Rev. Sci. Instrum. 72 (2001) 1143.
[26] L.L. Gurdev, T.N. Dreischuh, D.V. Stoyanov, J. Opt. Soc. Am. A 10 (1993) 2296.
[27] Ph. Salamitou, A. Dabas, P. Flamant, Appl. Opt. 34 (1995) 499.
[28] J.W. Goodman, in: J.C. Dainty (Ed.), Laser Speckle and Related Phenomena, Springer, Berlin, 1975, p. 9.
[29] J.H. Shapiro, B.A. Capron, R.C. Harney, Appl. Opt. 20 (1981) 3292.
[30] R.M. Hardesty, R.J. Keeler, M.J. Post, R.A. Richter, Appl. Opt. 20 (1981) 3763.
[31] P.H. Flamant, R.T. Menzies, M.J. Kavaya, Appl. Opt. 23 (1984) 1412.
[32] R.W. Hamming, Digital Filters, Prentice-Hall, Englewood Cliffs, NJ, 1983.
[33] T.N. Dreischuh, L.L. Gurdev, D.V. Stoyanov, in: P.A. Atanasov, S. Cartaleva (Eds.), Proceedings of SPIE, vol. 4397, 2001, pp. 481–485.
[34] G.N. Pearson, Rev. Sci. Instrum. 64 (1993) 1155.
[35] W.A. Brewer, R.M. Hardesty, in: Coherent Laser Radar, 1995 OSA Technical Digest Series, vol. 19, Optical Society of America, Washington, DC, 1995, p. 293.
[36] A. Finch, J.H. Flint, in: Coherent Laser Radar, 1995 OSA Technical Digest Series, vol. 19, Optical Society of America, Washington, DC, 1995, p. 310.

[37] C.J. Grund, in: Coherent Laser Radar, 1995 OSA Technical Digest Series, vol. 19, Optical Society of America, Washington, DC, 1995, p. 14.
[38] V. Wulfmeyer, M. Randall, C. Walther, R.K. Newsom, W.A. Brewer, R.M. Hardesty, in: A. Dabas, C. Loth, J. Pelon (Eds.), Advances in Laser Remote Sensing, Ecole Polytechnique, Palaiseau, France, 2000, p. 463.